

An estimation of the $^{18}\text{O}/^{16}\text{O}$ ratio of UT/LMS ozone based on artefact CO in air sampled during CARIBIC flights

S. Gromov¹, C. A. M. Brenninkmeijer¹

¹ Max Planck Institute for Chemistry, Mainz, Germany

Correspondence to: S. Gromov (sergey.gromov@mpic.de)

Abstract

An issue of O₃-driven artefact production of CO in the upper troposphere/lowermost stratosphere (UT/LMS) air analysed in the CARIBIC-1 project is being discussed. By confronting the CO mixing and isotope ratios obtained from different analytical instrumentation, we (i) reject natural/artificial sampling and mixing effects as possible culprits of the problem, (ii) ascertain the chemical nature and quantify the strength of the contamination, and (iii) demonstrate successful application of the isotope mass-balance calculations for inferring the isotope composition of the contamination source. The $\delta^{18}\text{O}$ values of the latter unambiguously indicate the oxygen being inherited from O₃. The $\delta^{13}\text{C}$ values hint at reactions of trace amounts of organics with stratospheric O₃ that could have yielded the artificial CO. While the exact contamination mechanism is not known, it is clear that the issue pertains only to the earlier (first) phase of the CARIBIC project. Finally, estimated UT/LMS ozone $\delta^{18}\text{O}$ values are lower than those observed in the stratosphere within the same temperature range, suggesting that higher pressures (240–270 hPa) imply lower isotope fractionation controlling the local $\delta^{18}\text{O}(\text{O}_3)$ value.

1 Introduction

[1] Accurate determination of the atmospheric carbon monoxide (CO) content based on the collection of air samples depends on the preservation of the mixing ratio of CO inside the receptacle, from the point of sampling to the moment of physicochemical analysis in a laboratory. A well known example in our field of research is the filling of pairs of glass flasks at South Pole

20 Station for analysis at NOAA in Boulder, Colorado, USA (Novelli *et al.*, 1998). There, the du-
21 plicate air sampling allowed for a degree of quality control which in view of the long transit
22 times, especially during polar winter, was a perhaps not perfect, but certainly a practical meas-
23 ure. Here we deal with a different case: Using aircraft-based collection of very large air samples
24 rendered duplicate sampling unpractical, yet analyses could be performed soon after the sam-
25 pling had taken place because of the proximity of the aircraft's landing location to the laborato-
26 ry involved. A presumption of the analytical integrity of the process was that the growth of CO
27 in receptacles is gradual and takes its time. Reminding Thomas Henry Huxley's statement, "The
28 great tragedy of Science – the slaying of a beautiful hypothesis by an ugly fact", it turned out,
29 however, that for air we collected in stainless steel tanks in the upper troposphere/lowermost
30 stratosphere (UT/LMS) higher CO values were measured in the laboratory than measured
31 *in situ* during the collection of these air samples. Moreover, measurement of the stable oxygen
32 isotopic composition of CO from these tanks revealed additional isotopic enrichments in ^{18}O of
33 10‰ or more. It was soon realised that this phenomenon was due to the formation of CO in
34 these tanks and/or possibly in the sampling system and inlet tubing used, by reactions involving
35 ozone (Brenninkmeijer *et al.*, 1999).

36 [2] Unexpectedly high $^{18}\text{O}/^{16}\text{O}$ ratios in stratospheric ozone (O_3) were discovered by Konrad
37 Mauersberger using a balloon-borne mass spectrometer (Mauersberger, 1981), which has trig-
38 gered a series of theoretical and experimental studies on atmospheric O_3 heavy isotope enrich-
39 ments (see, *e.g.*, Schinke *et al.* (2006) for a review). In view of the advances in theoretical and
40 laboratory studies on the isotopic composition of O_3 atmospheric measurements are welcome,
41 they do however form a challenge. In the stratosphere O_3 number concentrations are high, but
42 the remoteness of the sampling domain is a problem. In the troposphere, low O_3 number densi-
43 ties are the main obstacle, as indicated by few experiments performed to date
44 (Krankowsky *et al.*, 1995; Johnston and Thiemens, 1997; Vicars and Savarino, 2014). Never-
45 theless, recent analytical improvements, namely the use of an indirect method of reacting at-
46 mospheric O_3 with a substrate that can be analysed for the isotopic composition of the
47 O_3 -derived oxygen (Vicars *et al.*, 2012), has greatly improved our ability to obtain information
48 on the O_3 isotopic composition.

49 [3] Although the increase of CO concentrations in air stored in vessels is a well recognised
50 problem, to our knowledge a specific O_3 -related process has not been reported yet. Here we dis-
51 cuss this phenomenon and turn its disadvantage into an advantage, namely that of obtaining an
52 estimate of the oxygen isotopic composition of O_3 in the UT/LMS, an atmospheric domain not

53 yet covered by specific measurements. The air samples we examine in this study were collected
54 onboard a passenger aircraft carrying an airfreight container with analytical and air/aerosol
55 sampling equipment on long distance flights from Germany to South India and the Caribbean
56 within the framework of the CARIBIC project (Civil Aircraft for the Regular Investigation of
57 the atmosphere Based on an Instrument Container, <http://www.caribic-atmospheric.com>).

58 **2 Experimental and results**

2.1 Whole air sampling

59 [4] CARIBIC-1 (Phase #1, abbreviated hereafter “C1”) was operational from November 1998
60 until April 2002 using a *Boeing 767-300 ER* operated by LTU International Airlines
61 (Brenninkmeijer *et al.*, 1999). Using a whole air sample (WAS) collection system, twelve air
62 samples were collected per flight (of 8–10 hours duration at cruise altitudes of 10–12 km) in
63 stainless steel tanks for subsequent laboratory analysis of the mixing ratios (*i.e.* mole fractions)
64 of various trace gases, including ^{14}CO . Large air samples were required in view of the ultra-low
65 number density of this mainly cosmogenic tracer (10–100 molecules cm^{-3} standard temperature
66 and pressure (STP), about 0.4–4 amol/mol). Hereinafter STP denotes dry air at 273.15 K,
67 101325 Pa. Each C1 WAS sample (holding 350 litres of air STP) was collected over 15–20 min
68 intervals representing the number density-weighted average of the compositions encountered
69 along flight segments of about 250 km. The overall uncertainty of the measured WAS CO is
70 less than $\pm 1\%$ for the mixing ratio and $\pm 0.1\text{‰}/\pm 0.2\text{‰}$ for $\delta^{13}\text{C}(\text{CO})/\delta^{18}\text{O}(\text{CO})$, respectively
71 (Brenninkmeijer, 1993; Brenninkmeijer *et al.*, 2001). Isotope compositions are reported
72 throughout this manuscript using the so-called delta value $\delta = (R/R_{\text{st}} - 1)$ relating the ratio R of
73 rare (^{13}C , ^{18}O or ^{17}O) over abundant isotopes of interest to the standard ratio R_{st} . These are Vi-
74 enna Standard Mean Ocean Water (VSMOW) for $^{18}\text{O}/^{16}\text{O}$ (Gonfiantini, 1978; Coplen, 1994)
75 and $^{17}\text{O}/^{16}\text{O}$ (Assonov and Brenninkmeijer, 2003), and Vienna Pee Dee Belemnite (VPDB) for
76 $^{13}\text{C}/^{12}\text{C}$ (Craig, 1957), respectively. As we mention above, the oxygen isotope composition of
77 the CO present in these WAS samples was corrupted, in particular when O_3 levels were as high
78 as 100–600 nmol/mol.

79 [5] CARIBIC-2 (Phase #2, referred to as “C2”) started operation in December 2004 with a
80 Lufthansa *Airbus A340-600* fitted with a new inlet system and air sampling lines, including per-
81 fluoroalkoxy alkane (PFA) lined tubing for trace gas intake (Brenninkmeijer *et al.*, 2007). No
82 flask CO mixing/isotope ratio measurements are performed in C2.

2.2 On-line instrumentation

83 [6] In addition to the WAS collection systems, both C1 and C2 measurement setups include dif-
84 ferent instrumentation for on-line detection of [CO] and [O₃] (hereinafter the squared brackets
85 [] denote the mixing ratio of the respective species). *In situ* CO analysis in C1 is done using a
86 gas chromatography (GC)-reducing gas analyser which provides measurements every 130 s
87 with an uncertainty of ± 3 nmol/mol (Zahn *et al.*, 2000). In C2, a vacuum ultraviolet fluores-
88 cence (VUV) instrument with lower measurement uncertainty and higher temporal resolution of
89 ± 2 nmol/mol in 2 s (Scharffe *et al.*, 2012) is employed. Furthermore, the detection frequency
90 for O₃ mixing ratios has also increased, *viz.*, from 0.06 Hz in C1 to 5 Hz in C2
91 (Zahn *et al.*, 2002; Zahn *et al.*, 2012).

2.3 Results

92 [7] When comparing the CO mixing ratios in relation to those of O₃ for C1 and C2, differences
93 are apparent in the LMS, where C2 [CO] values are systematically lower. This is illustrated in
94 Fig. 1 (a) which presents the LMS CO-O₃ distribution of the C2 *in situ* measurements overlaid
95 with the C1 *in situ* and WAS data. The entire C1 CO/O₃ dataset is presented in Fig. 2. For the
96 *in situ* CO datasets we calculated the statistics (Fig. 1 (b)) of the samples with respective O₃
97 mixing ratios clustered in 20 nmol/mol bins, *i.e.* the median and spread of [CO] as a function of
98 [O₃] analysed. The interquartile range, IQR, is used in the current analysis as a robust measure
99 of the data spread instead of the standard deviation. The data exhibit large [CO] variations at
100 [O₃] below 400 nmol/mol that primarily reflect pronounced seasonal variations in the NH tropo-
101 spheric CO mixing ratio. With increasing [O₃], [CO] decreases to typical stratospheric values,
102 and its spread reduces to mere 3.5 nmol/mol and less, as [O₃] surpasses 500 nmol/mol. Despite
103 the comparable spread in C1 and C2 [CO], from 400 nmol/mol of [O₃] onwards the C1 CO mix-
104 ing ratios start to level off, with no samples below 35 nmol/mol having been detected, whereas
105 the C2 levels continuously decline. By the 580 nmol/mol O₃ bin, C1 [CO] of $39.7^{+0.3}$ nmol/mol
106 contains some extra 14 nmol/mol compared to $25.6^{+1.7}$ nmol/mol typical for C2 values. Overall,
107 at [O₃] above 400 nmol/mol the conspicuously high [CO] is marked in about 200 *in situ* C1
108 samples, of which 158 and 69 emerge as statistically significant mild and extreme outliers, re-
109 spectively, when compared against the number of C2 samples ($n > 3 \cdot 10^5$). The conventions here
110 follow Natrella (2003), *i.e.* ± 1.5 and ± 3 IQR ranges define the inner and outer statistical fences
111 (ranges outside which the data points are considered mild and extreme outliers) of the C2 [CO]
112 distribution in every O₃ bin, respectively. The statistics include the samples in bins with average

113 [O₃] of 420–620 nmol/mol. None of C1 CO at [O₃] above 560 nmol/mol agrees with the C2 ob-
114 servations. Because the CO-O₃ distribution cannot have changed over the period in question, we
115 find that an apparent relative excess CO of up to 55% justifies and investigation into sampling
116 artefacts and calibration issues.

117 [8] Unnatural elevations in $\delta^{18}\text{O}(\text{CO})$ from WAS measurements are also evident, as shown in
118 Figs. 3 and 4. The large $\delta^{18}\text{O}(\text{CO})$ elevations that reach beyond +16‰ are found to be propor-
119 tional to the concomitant O₃ mixing ratios (denoted with colour) and are more prominent at
120 lower [CO]. Lower $\delta^{18}\text{O}(\text{CO})$ values, however, are expected based on our knowledge of UT/
121 LMS CO sources (plus their isotope signatures) and available *in situ* observations (Fig. 3,
122 shown with triangles), as elucidated by Brenninkmeijer *et al.* (1996) (hereafter denoted as
123 “B96”). That is, the greater the proportion of stratospheric CO, the greater its fraction stemming
124 from methane oxidation with a characteristic $\delta^{18}\text{O}$ of 0‰ or lower (Brenninkmeijer and Röck-
125 mann, 1997). This occurs because the CO sink at ruling UT/LMS temperatures proceeds more
126 readily than its production, as the reaction of hydroxyl radical (OH) with CO, being primarily
127 pressure-dependent, is faster than the temperature-sensitive reaction of OH with CH₄. Further-
128 more, as the lifetime of CO quickly decreases with altitude, transport-mixing effects take the
129 lead in determining the vertical distributions of [CO] and $\delta^{18}\text{O}(\text{CO})$ above the tropopause,
130 hence their mutual relationship. This is seen from the B96 data at [CO] below 50 nmol/mol that
131 line-up in a near linear relationship towards the end-members with lowest ¹⁸O/¹⁶O ratios. These
132 result from the largest share of the ¹⁸O-depleted photochemical component and extra depletion
133 caused by the preferential removal of C¹⁸O in reaction with OH (fractionation about +11‰ at
134 pressures below 300 hPa, Stevens *et al.*, 1980; Röckmann *et al.*, 1998b).

135 [9] We are confident that the enhancements of C1 C¹⁸O originate from O₃, whose large enrich-
136 ment in ¹⁸O (above +60‰ in $\delta^{18}\text{O}$, Brenninkmeijer *et al.*, 2003) is typical and found transferred
137 to other atmospheric compounds (see Savarino and Morin (2012) for a review). In Fig. 3 it is al-
138 so notable that not only the LMS compositions are affected but elevations of (3–10)‰ from the
139 bulk $\delta^{18}\text{O}(\text{CO})$ values are present in more tropospheric samples with [CO] of up to
140 100 nmol/mol. These result from the dilution of the least affected CO-rich tropospheric air by
141 CO-poor, however substantially contaminated, stratospheric air, sampled into the same WAS
142 tank. Such sampling-induced mixing renders an unambiguous determination of the artefact
143 source’ isotope signature rather difficult, because neither mixing nor isotope ratios of the ad-
144 mixed air portions are known sufficiently well (see below).

145 [10] Differences between the WAS and *in situ* measured [CO] – a possible indication that the
146 $\delta^{18}\text{O}(\text{CO})$ contamination pertains specifically to the WAS data – average at $\bar{\Delta}(\text{WAS}-\textit{in situ}) =$
147 (5.3 ± 0.2) nmol/mol (± 1 standard deviation of the mean, $n = 408$) and happen to be random with
148 respect to any operational parameter or measured characteristic in C1, *i.e.* irrespective of CO or
149 O_3 abundances. The above mentioned discrepancy remained after several calibrations between
150 the two systems had been performed, and likely results from the differences in the detection
151 methods, drifts of the calibration standards used (see details in Brenninkmeijer *et al.*, 2001) and
152 a short-term production of CO in the stainless steel tanks during sampling. The large spread of
153 $\Delta(\text{WAS}-\textit{in situ})$ of ± 3.5 nmol/mol ($\pm 1\sigma$ of the population) ensues from the fact that the *in situ*
154 sampled air corresponds to (2–4)% of the concomitantly sampled WAS volume, as typically
155 6–7 *in situ* collections of 5 s were made throughout one tank collection of 17–21 min. The in-
156 tegrity of the WAS CO is further affirmed by the unsystematic distribution of the artefact com-
157 positions among tanks (in contrast to that for $\delta^{18}\text{O}(\text{CO}_2)$ in C1 discussed by As-
158 sonov *et al.*, 2009). Overall, the WAS and *in situ* measured CO mixing ratios correlate extreme-
159 ly well (adj. $R^2 = 0.972$, slope of 0.992 ± 0.008 ($\pm 1\sigma$), $n = 408$). However, both anomalies in
160 [CO] and $\delta^{18}\text{O}(\text{CO})$ manifest clear but complex influences of the concomitant [O_3]. That is, the
161 C1 *in situ* and WAS data very likely evidence artefacts pertaining to the O_3 -driven effect of the
162 same nature. Below we discuss and quantify these influences.

163 3 Discussion

164 [11] Three factors may lead to the (artefact) distributions seen for C1 *in situ* [CO] at LMS O_3
165 mixing ratios, namely:

166 [12] (i) Strong (linear) natural mixing, such as enhanced stratosphere-troposphere exchange
167 (STE), when a [CO] outside the statistically expected range results from the integration of air
168 having dissimilar ratios of the tracers' mixing ratios, *viz.* [O_3]:[CO]. For example, mixing of
169 two air parcels in a 16%:84% proportion (by moles of air) with typical [O_3]:[CO] of 700:24
170 (stratospheric) and 60:125 (tropospheric), respectively, yields an integrated composition with
171 [O_3]:[CO] of 598:40 which indeed corresponds to C1 data (this case is exemplified by the mix-
172 ing curve in Fig. 1). Nonetheless, occurrences of rather high stratospheric CO mixing ratios (in
173 our case, 40 nmol/mol at the concomitant [O_3] of 500–600 nmol/mol compared to the typical
174 24–26 nmol/mol) are rare. For instance, a deep STE similar to that described by
175 Pan *et al.* (2004) was observed by C2 only once (*cf.* the outliers at [O_3] of 500 nmol/mol in
176 Fig. 1), whereas the C1 outliers were exclusively registered in some 12 flights during

177 1997–2001. No relation between these outliers and the large-scale [CO] perturbation due to ex-
178 tensive biomass burning in 1997/1998 (Novelli *et al.*, 2003) is established, otherwise elevated
179 CO mixing ratios should manifest themselves at lower [O₃] as well. Other tracers detected in
180 CARIBIC provide supporting evidence against such strongly STE-mixed air having been cap-
181 tured by C1. That is, the binned distributions for water vapour and de-trended N₂O mixing rati-
182 os (not shown here) are similar for C1 and C2. Whereas the small relative variations in atmos-
183 pheric [N₂O] merely confirm matching [O₃] distributions in CARIBIC, the stratospheric [H₂O]
184 distributions witness no [O₃]:[H₂O] values corresponding to those of the C1 outliers, suggesting
185 the latter being unnaturally low.

186 [13] (ii) Mixing effects can also occur artificially, originating from sampling peculiarities or data
187 processing. Since the CARIBIC platform is not stationary, about 5 s long sampling of an *in situ*
188 air probe in C1 implies integration of the air compositions encountered along some hundred me-
189 tres, owing to the high aircraft speed. This distance may cover a transect between tropospheric
190 and stratospheric filaments of different compositions. The effect of such ‘translational mixing’
191 can be simulated by averaging the sampling data with higher temporal frequency over longer
192 time intervals. In this respect, the substantially more frequent CO data in C2 (sampling interval
193 <1 s) were artificially averaged over a set of increasing intervals to reckon whether the long
194 sampling period in C1 could be the culprit for skewing its CO–O₃ distribution. As a result, the
195 original C2 data and their averages (equivalent to the C1 CO sample injection time) differ neg-
196 ligibly, as do the respective [O₃]:[CO] values. Our simulations of the ‘translational mixing’ ef-
197 fects confirm that the actual C2 CO–O₃ distribution in the region of interest ([O₃] of
198 540–620 nmol/mol) remains insensitive to averaging intervals of up to 300 s. Furthermore, a
199 very strong artificial mixing with an averaging interval of at least 1200 s (comparable to C1
200 WAS sampling time) is required to yield the averages from the C2 data with [O₃]:[CO] charac-
201 teristic for the C1 outliers.

202 [14] (iii) In view of the above, it is unlikely that any natural or artificial mixing processes are in-
203 volved in the stratospheric [CO] discrepancies seen in C1. We therefore conclude that the sam-
204 ple contamination in C1 occurred prior to the probed air reaching the analytical instrumentation
205 and WAS sampling tanks in the container, since clearly elevated stratospheric CO mixing ratios
206 are common to WAS and *in situ* data. Two more indications, *viz.* growing [CO] discrepancy
207 with increasing O₃ abundance, and the strong concomitant signal in δ¹⁸O(CO), suggest that O₃-
208 mediated production of CO took place. Further, by confronting the C1 and C2 [CO] measure-

209 ments in a regression analysis (detailed in Appendix A), we quantify the artefact component
 210 $[\text{CO}]_c$ being chiefly a function of O_3 mixing ratio as

$$[\text{CO}]_c = b \cdot [\text{O}_3]^2, \quad b = (5.19 \pm 0.12) \cdot 10^{-5} \text{ [mol/nmol]}, \quad (1)$$

211 which is equivalent to 8–18 nmol/mol throughout the respective $[\text{O}_3]$ range of
 212 400–620 nmol/mol (see Fig. 1 (d)). Subtracting this artefact signal yields the corrected *in situ*
 213 C1 CO– O_3 distribution conforming to that of C2 (*cf.* red symbols in Fig. 1 (a)).

214 [15] Importantly, since we can quantify the contamination strength using only the O_3 mixing ra-
 215 tio, the continuous *in situ* C1 $[\text{O}_3]$ data allow estimating the integral artefact CO component in
 216 each WAS sample and, if the isotope ratio of contaminating O_3 is known, to derive the initial
 217 $\delta^{18}\text{O}(\text{CO})$. The latter, as it was mentioned above, is subject to strong sample-mixing effects,
 218 which is witnessed by $\delta^{18}\text{O}(\text{CO})$ outliers even at relatively high $[\text{CO}]$ up to 100 nmol/mol. Ac-
 219 counting for such cases is, however, problematic since it is necessary to distinguish the propor-
 220 tions of the least modified (tropospheric) and significantly affected (stratospheric) components
 221 in the resultant WAS sample mix. Since this information is not available, we applied an *ad hoc*
 222 correction approach, as described in the following. This approach is capable of determining the
 223 contamination source (*i.e.*, O_3) isotope signature as well.

3.1 Contamination isotope signatures

224 [16] We use the differential mixing model (MM, originally known as the “Keeling-plot”), be-
 225 cause it requires only the estimate of the artefact component mixing ratio, but no assumptions
 226 on the (unknown) shares and isotope signatures of the air portions mixed in a given WAS tank.
 227 The MM parameterises the admixing of the portion of artefact CO to the WAS sample with the
 228 “true” initial composition, as formulated below:

$$[\text{CO}]_a = [\text{CO}]_t + [\text{CO}]_c, \quad (2)$$

$${}^i\delta_a [\text{CO}]_a = {}^i\delta_t [\text{CO}]_t + {}^i\delta_c [\text{CO}]_c, \quad (3)$$

229 where indices a , c and t distinguish the mixing ratios and isotope compositions ${}^i\delta$ (${}^{18}\delta$ and ${}^{13}\delta$
 230 for ${}^{13}\text{C}$ and ${}^{18}\text{O}$, respectively) pertaining to the analysed sample, estimated contamination and
 231 “true” composition sought (*i.e.*, $[\text{CO}]_t$ and ${}^i\delta_t$), respectively. Here the contamination strength
 232 $[\text{CO}]_c$ is derived by integrating Eq. (1) using the *in situ* C1 $[\text{O}_3]$ data for each WAS sample. By
 233 rewriting the above equation with respect to the isotope signature of the analysed CO, one ob-
 234 tains:

$${}^i\delta_a = {}^i\delta_c + ({}^i\delta_t - {}^i\delta_c) [\text{CO}]_c / [\text{CO}]_a, \quad (4)$$

235 which signifies that linear regression of ${}^i\delta_a$ as a function of the reciprocal of $[\text{CO}]_a$ yields the es-
236 timated contamination signature ${}^i\delta_c$ at $([\text{CO}]_a)^{-1} \rightarrow 0$ when invariable "true" compositions
237 ($[\text{CO}]_t, {}^i\delta_t$) are taken (the Keeling plot detailing these calculations is shown in Fig. 5). We there-
238 fore apply the MM described by Eq. (4) to the subsets of samples picked according to the same
239 reckoned $[\text{CO}]_t$ (within a ± 2 nmol/mol window, $n > 7$). Such selection, however, may be insuf-
240 ficient: Due to the strong sampling effects in the WAS samples (see previous Section), it is pos-
241 sible to encounter samples that integrate different air masses to the same $[\text{CO}]_t$ but rather differ-
242 ent average ${}^i\delta_t$. The solution in this case is to refer to the goodness of the MM regression fit, be-
243 cause the R^2 intrinsically measures the linearity of the regressed data, *i.e.* closeness of the "true"
244 values in a regarded subset of samples, irrespective of underlying reasons for that.

245 [17] Higher R^2 values thus imply higher consistency of the estimate, as demonstrated in Fig. 6
246 showing the calculated ${}^i\delta_c$ for $[\text{CO}]_t$ below 80 nmol/mol as a function of the regression R^2 . The
247 latter decreases with greater $[\text{CO}]_t$ (*i.e.*, larger sample subset size, since tropospheric air is more
248 often encountered) and, correspondingly, larger variations in ${}^i\delta_t$. Ultimately, at lower R^2 the in-
249 ferred ${}^{18}\delta_c$ converge to values slightly above zero expected for uncorrelated data, *i.e.* C1
250 $\delta^{18}\text{O}(\text{CO})$ tropospheric average. A similar relationship is seen for the ${}^{13}\delta_c$ values (they converge
251 around -28‰), however, there are no consistent estimates found (R^2 is generally below 0.4).
252 Since such is not the case for $\delta^{18}\text{O}$, the MM is not sufficiently sensitive to the changes caused
253 by the contamination, which implies that the artefact CO $\delta^{13}\text{C}$ should be within the range of the
254 "true" $\delta^{13}\text{C}(\text{CO})$ values. Interestingly, the MM is rather responsive to the growing fraction of
255 the CH_4 -derived component in CO with increasing $[\text{O}_3]$, as the ${}^{13}\delta_c$ value of $-(47.2 \pm 5.8)\text{‰}$ in-
256 ferred at R^2 above 0.4 is characteristic for the $\delta^{13}\text{C}$ of methane in the UT/LMS. It is important to
257 note that we have accounted for the biases in the analysed C1 WAS $\delta^{13}\text{C}(\text{CO})$ expected from
258 the mass-independent isotope composition of O_3 (see details in Appendix B).

259 [18] We derive the "best-guess" estimate of the admixed CO ${}^{18}\text{O}$ signature at ${}^{18}\delta_c =$
260 $+(92.0 \pm 8.3)\text{‰}$, which agrees with the other MM results obtained at R^2 above 0.75. Taking the
261 same subsets of samples, the concomitant ${}^{13}\text{C}$ signature matches ${}^{13}\delta_c = -(23.3 \pm 8.6)\text{‰}$, indeed at
262 the upper end of the expected LMS $\delta^{13}\text{C}(\text{CO})$ variations of $-(25-31)\text{‰}$. Because of that, the
263 MM is likely insensitive to the changes in $\delta^{13}\text{C}(\text{CO})$ caused by the contamination (the corre-
264 sponding R^2 values are below 0.1). Upon the correction using the inferred ${}^{18}\delta_c$ value, the C1
265 WAS $\delta^{18}\text{O}(\text{CO})$ data agree with B96 (shown with red symbols in Fig. 3). That is, variations in
266 the observed C^{18}O are driven by (i) the seasonal/regional changes in the composition of tropo-
267 spheric air and by (ii) the degree of mixing or replacement of the latter with the stratospheric

268 component that is less variable in ^{18}O . This is seen as stretching of the scattered tropospheric
269 values ($[\text{CO}]$ above 60 nmol/mol) towards $\delta^{18}\text{O}(\text{CO})$ of around -10‰ at $[\text{CO}]$ of 25 nmol/mol,
270 respectively. The corrected C1 $\delta^{13}\text{C}(\text{CO})$ data (shown in Fig. 7) are found to be in a $\pm 1\text{‰}$
271 agreement with the observations by B96, except for several deep stratospheric samples ($[\text{CO}]$
272 below 40 nmol/mol). The latter were encountered during “ozone hole” conditions and carried
273 extremely low $\delta^{13}\text{C}(\text{CO})$ values, which was attributed to the reaction of methane with available
274 free Cl radicals (Brenninkmeijer *et al.*, 1996).

3.2 Estimate of $\delta^{18}\text{O}(\text{O}_3)$

275 [19] The contamination ^{18}O signature inferred here ($^{18}\delta_c = +(92.0 \pm 8.3)\text{‰}$) likely pertains to O_3
276 and is comparable to $\delta^{18}\text{O}(\text{O}_3)$ values measured in the stratosphere at temperatures about 30 K
277 lower than those encountered in the UT/LMS by C1 (see Table 1 for comparison). If no other
278 factors are involved (see below), this discrepancy in $\delta^{18}\text{O}(\text{O}_3)$ should be attributed to the local
279 conditions, *i.e.* the higher pressures (typically 240–270 hPa for C1 cruising altitudes) at which
280 O_3 was formed. Indeed, the molecular lifetime (the period through which the species’ isotope
281 reservoir becomes entirely renewed, as opposed to the “bulk” lifetime) of O_3 encountered along
282 the C1 flight routes is estimated on the order of minutes to hours at daylight (H. Riede, Max
283 Planck Institute for Chemistry, 2010), thus the isotope composition of the photochemically re-
284 generated O_3 resets quickly according to the local conditions. Virtual absence of sinks, in turn,
285 leads to “freezing” of the $\delta^{18}\text{O}(\text{O}_3)$ value during night in the UT/LMS. Verifying the current
286 $\delta^{18}\text{O}(\text{O}_3)$ estimate against the kinetic data, in contrast to the stratospheric cases, is problematic.
287 The laboratory studies on O_3 formation to date have scrutinised the concomitant kinetic isotope
288 effects (KIEs) as a function of temperature at only low pressures (67 mbar); the attenuation of
289 the KIEs with increasing pressure was studied only at room temperatures (see Table 1, also
290 Brenninkmeijer *et al.* (2003) for references). A rather crude attempt may be undertaken by as-
291 suming that the formation KIEs become attenuated at higher pressures in a similar (proportion-
292 al) fashion to that measured at 320 K, however applied to the nominal low-pressure values
293 reckoned at (220–230) K. A decrease in $\delta^{18}\text{O}(\text{O}_3)$ of about (6–8) ‰ is expected from such cal-
294 culation (*cf.* last row in Table 1), yet accounting for a mere one-half of the (13–15) ‰ discrep-
295 ancy between the stratospheric $\delta^{18}\text{O}(\text{O}_3)$ values and $^{18}\delta_c$.

296 [20] Lower $^{18}\delta_c$ values could result from possible isotope fractionation accompanying the pro-
297 duction of the artefact CO. Although not quantifiable here, oxygen KIEs in the $\text{O}_3 \rightarrow \text{CO}$ con-
298 version chain cannot be ruled out, recalling that the intermediate reaction steps are not identifi-

299 able and the artefact CO represents at most 4% of all O₃ molecules. Furthermore, the yield λ_{O_3}
300 of CO from O₃ may be lower than unity (see details in Appendix A). On the other hand, the in-
301 ference that the contamination strength primarily depends on [O₃] indicates that the kinetic frac-
302 tionation may have greater effect on the carbon isotope ratios of the artefact CO produced (the
303 $^{13}\delta_c$ values) in contrast to the oxygen ones. That is because all reactive oxygen available from
304 O₃ becomes converted to CO, whilst the concomitant carbon atoms are drawn from a virtually
305 unlimited pool whose apparent isotope composition is altered by the magnitude of the ^{13}C KIEs.

306 [21] Besides KIEs, selectivity in the transfer of O atoms from O₃ to CO affects the resulting $^{18}\delta_c$
307 value. The terminal O atoms in O₃ are enriched with respect to the molecular (bulk) O₃ compo-
308 sition when the latter is above +70‰ in $\delta^{18}\text{O}$ (Janssen, 2005; Bhattacharya *et al.*, 2008), there-
309 fore an incorporation of only central O atoms into the artefact CO molecules should result in a
310 reduced apparent $^{18}\delta_c$ value. Such exclusive selection is, however, less likely from the kinetic
311 standpoint and was not observed in available laboratory studies (see Savarino *et al.* (2008) for a
312 review). For instance, Röckmann *et al.* (1998a) established the evidence of direct O transfer
313 from O₃ to the CO produced in alkene ozonolysis. A reanalysis of their results (in light of find-
314 ings of Bhattacharya *et al.* (2008)) suggests that usually the terminal atoms of the O₃ molecule
315 become transferred (their ratio over the central ones changes from the bulk 2:1 to 1:0 for vari-
316 ous species). Considering the alternatives of the O transfer in our case (listed additionally in
317 Table 1), the equiprobable incorporation of the terminal and central O₃ atoms into CO should
318 result in the $\delta^{18}\text{O}(\text{O}_3)$ value in agreement with the “crude” estimate based on laboratory data
319 given above.

320 [22] Furthermore, the conditions that supported the reaction of O₃ (or its derivatives) followed by
321 the production of CO are vague. A few hypotheses ought to be scrutinised here. First, a fast
322 O₃ → CO conversion must have occurred, owing to short (*i.e.*, fraction of a second) exposure
323 time of the probed air to the contamination. Accounting for the typical C1 air sampling condi-
324 tions (these are: sampled air pressure of 240–270 hPa and temperature of 220–235 K outboard
325 to 275–300 K inboard, sampling rate of $12.85 \cdot 10^{-3} \text{ mol s}^{-1}$ corresponding to 350 L STP sam-
326 pled in 1200 s, inlet/tubing volume gauged to yield exposure times of 0.01 to 0.1 s due to varia-
327 ble air intake rate, [O₃] of 600 nmol/mol), the overall reaction rate coefficient (k_c in Eq. (A3)
328 from Appendix A) must be on the order of $(6 \cdot 10^{-15} / \tau_c) \text{ molecules}^{-1} \text{ cm}^3$, where τ_c is the exposure
329 time. Assuming the case of a gas-phase CO production from a recombining O₃ derivative and
330 an unknown carbonaceous compound X, the reaction rate coefficient for the latter (k in Eq. (A2)
331 in Appendix A) must be unrealistically high, at least $6 \cdot 10^{-10} \text{ molec}^{-1} \text{ cm}^3 \text{ s}^{-1}$ over $\tau_c = 1/100 \text{ s}$.

332 This number decreases proportionally with growing τ_c and $[X]$, if we take less strict exposure
333 conditions. Nonetheless, in order to provide the amounts of artefact CO we detect, a minimum
334 mixing ratio of 20 nmol/mol (or up to 4 μg of C per flight) of X is required, which is not availa-
335 ble in the UT/LMS from the species readily undergoing ozonolysis, *e.g.* alkenes.

336 [23] Second, a more complex heterogeneous chemistry on the inner surface of the inlet or sup-
337 plying tubing may be involved. Such can be the tracers' surface adsorption, (catalytic) decom-
338 position of O_3 and its reaction with organics or with surface carbon that also may lead to the
339 production of CO (Oyama, 2000). Evidence exists for the dissociative adsorption of O_3 on the
340 surfaces with subsequent production of the reactive atomic oxygen species (see, *e.g.*,
341 Li *et al.*, 1998, also Oyama, 2000). It is probable that sufficient amounts of organics have re-
342 mained on the walls of the sampling line exposed to highly polluted tropospheric air, to be later
343 broken down by the products of the heterogeneous decomposition of the ample stratospheric O_3 .
344 Unfortunately, the scope for a detailed quantification of intricate surface effects in the C1 CO
345 contamination problem is very limited.

346 4 Conclusions

347 [24] Recapitulating, the *in situ* measurements of CO and O_3 allowed us to unambiguously quanti-
348 fy the artefact CO production from O_3 likely in the sample line of the CARIBIC-1 instrumenta-
349 tion. Strong evidence to that is provided by the isotope CO measurements. We demonstrate the
350 ability of the simple mixing model ("Keeling-plot" approach) to single out the contamination
351 isotope signatures even in the case of a large sampling-induced mixing of the air with very dif-
352 ferent compositions. Obtained as a collateral result, the estimate of the $\delta^{18}\text{O}(\text{O}_3)$ in the UT/LMS
353 appears adequate, calling, however, for additional laboratory data (*e.g.*, the temperature-driven
354 variations of the O_3 formation KIE at pressures above 100 hPa) for a more unambiguous verifi-
355 cation.

356 Appendix A. Contamination assessment

357 [25] We quantify the C1 CO contamination strength (denoted $[\text{CO}]_c$, obtained by discriminating
358 the C1 outliers from respective C2 data) in a sequence of regression analyses. We foremost as-
359 certain that no other species or operational parameter (*e.g.* temperature, pressure, flight dura-
360 tion, season, latitude, time of day, *etc.*) measured in C1 appear to determine (*e.g.*, systematically
361 correlate with) $[\text{CO}]_c$, except that for $[\text{O}_3]$. We hypothesise therefore that a production of arte-

362 fact CO molecules was initiated by O₃ (via either its decomposition or a reaction with an un-
 363 known educt) and proceeded with incorporation of carbon (donated by some carbonaceous spe-
 364 cies X) and oxygen (donated by O₃ or its derivatives) atoms into final CO. Despite that neither
 365 the actual reaction chain nor its intermediates are known, it is possible to describe the artefact
 366 CO component produced (hereinafter curly brackets {} denote number densities) as

$$\{\text{CO}\}_c = \lambda_{\text{O}_3} \nu \tau_c, \quad (\text{A1})$$

367 where the yield λ_{O_3} , a diagnostic quantity, relates the amount of artefact CO molecules produced
 368 to the total number of O₃ molecules consumed in the system, τ_c denotes the reaction time (peri-
 369 od throughout which sampled air is exposed to contamination), and ν stands for the overall rate
 370 of the reaction chain. The latter, being regarded macroscopically (empirically), is parameterised
 371 to account for the order of reaction chain rate with respect to hypothesised reactants
 372 (McNaught and Wilkinson, 1997) as

$$\nu = k \{\text{X}\}^K \{\text{O}_3\}^\kappa, \quad (\text{A2})$$

373 where κ and K are the partial orders with respect to X and O₃ number densities, respectively,
 374 and k is the rate coefficient. Here it is implied that changes to $\{\text{X}\}$ and $\{\text{O}_3\}$ are negligible
 375 throughout the exposure time τ_c (typically < 0.1 s for C1 sample line). As stated above, we find
 376 that variations in $\{\text{CO}\}_c$ correlate exclusively with variations in $\{\text{O}_3\}$, hence Eq. (A2) can be
 377 reduced by assuming constancy of $\{\text{X}\}$ and K to:

$$\nu_c = k_c \{\text{O}_3\}^\kappa. \quad (\text{A3})$$

378 Here, $k_c = k \{\text{X}\}^K$ (often referred to as pseudo-first-order or “observed” rate coefficient) quanti-
 379 fies the rate of reaction chain exclusively propelled by O₃. Finally, using Eqs. (A1) and (A3),
 380 the artefact $\{\text{CO}\}_c$ component is expressed as

$$\{\text{CO}\}_c = b \cdot \{\text{O}_3\}^\kappa, \quad b = \lambda_{\text{O}_3} k_c \tau_c \quad (\text{A4})$$

381 where the constant proportionality factor b integrates the influence of the unknown (and as we
 382 explicate below, likely invariable) $\{\text{X}\}$, k , K and τ_c .

383 [26] Eq. (A4) defines the regression expression using which we attempt to fit the values of
 384 $\{\text{CO}\}_c$ as a function of κ , $\{\text{O}_3\}$ and b . In the first regression iteration we keep both κ and b
 385 as free parameters, which provides best approximation at $\kappa = 2.06 \pm 0.38$, suggesting reactions of
 386 two O₃ molecules in case elementary reactions constitute the reaction mechanism, or two ele-
 387 mentary steps involving O₃ or its derivatives in case a stepwise reaction is involved
 388 (McNaught and Wilkinson, 1997). In a subsequent regression iteration we set $\kappa = 2$, which
 389 yields better (as opposed to the first iteration) estimate of b of $(5.19 \pm 0.12) \cdot 10^{-5}$ mol/nmol ($\pm 1\sigma$,

390 adj. $R^2 = 0.83$, red. $\chi^2 = 4.0$; here the value of b in mole fraction units is derived using the air
391 density at C1 sampling conditions for relating fitted $[\text{CO}]_c$ and observed $[\text{O}_3]^2$). At last, we as-
392 certain that the best regression results are obtained particularly at $\kappa = 2$, as indicated by the re-
393 gression statistic (R^2 and χ^2) that asymptotically improves when a set of regressions with neigh-
394 bouring (*i.e.* below and above 2) integer values of κ is compared. The low uncertainty (within
395 $\pm 3\%$) associated with the estimate of b confirms an exclusive dependence of the contamination
396 source on the O_3 mixing ratio, as well as much similar reaction times τ_c . The regressed value of
397 $[\text{CO}]_c$ as a function of $[\text{O}_3]$ is presented in Fig. 1 (d) (solid line). It is possible to constrain the
398 overall yield λ_{O_3} of CO molecules in the artefact source chain to be between 0.5 and 1, compar-
399 ing the magnitude of $[\text{CO}]_c$ to the discrepancy between the $[\text{O}_3]$ measured in C1 and C2
400 (± 20 nmol/mol, taken equal to the $[\text{O}_3]$ bin size owing to the $\text{N}_2\text{O}-\text{O}_3$ and $\text{H}_2\text{O}-\text{O}_3$ distributions
401 matching well between the datasets). Lower λ_{O_3} values, otherwise, should have resulted in a no-
402 ticeable (*i.e.*, greater than 20 nmol/mol) decrease in the C1 O_3 mixing ratios with respect to the
403 C2 levels.

404 **Appendix B. Corrections to measured $\delta^{13}\text{C}(\text{CO})$ values due to the oxygen**

405 **MIF**

406 [27] Atmospheric O_3 carries an anomalous isotope composition (or mass-independent fractiona-
407 tion, MIF) with a substantially higher relative enrichment in ^{17}O over that in ^{18}O (above $+25\%$
408 in $\Delta^{17}\text{O} = (\delta^{17}\text{O}+1)/(\delta^{18}\text{O}+1)^\beta - 1$, $\beta = 0.528$) when compared to the majority of terrestrial oxy-
409 gen reservoirs that are mass-dependently fractionated (*i.e.*, with $\Delta^{17}\text{O}$ of 0%) (see Brenninkmeij-
410 er *et al.* (2003) and refs. therein). CO itself also has an unusual oxygen isotopic composition,
411 possessing a moderate tropospheric MIF of around $+5\%$ in $\Delta^{17}\text{O}(\text{CO})$ induced by the sink KIEs
412 in reaction of CO with OH (Röckmann *et al.*, 1998b; Röckmann *et al.*, 2002) and a minor
413 source effect from the ozonolysis of alkenes (Röckmann *et al.*, 1998a; Gromov *et al.*, 2010). A
414 substantial contamination of CO by O_3 oxygen induces proportional changes to $\Delta^{17}\text{O}(\text{CO})$ that
415 largely exceed its natural atmospheric variation. On the other hand, the MIF has implications in
416 the analytical determination of $\delta^{13}\text{C}(\text{CO})$, because the presence of C^{17}O species interferes with
417 the mass-spectrometric measurement of the abundances of ^{13}CO possessing the same basic mo-
418 lecular mass (m/z is 45). When inferring the exact $\text{C}^{17}\text{O}/\text{C}^{18}\text{O}$ ratio in the analysed sample is not
419 possible, analytical techniques usually involve assumptions (*e.g.*, mass-dependently fractionated
420 compositions or a certain non-zero $\Delta^{17}\text{O}$ value) with respect to the C^{17}O abundances
421 (Assonov and Brenninkmeijer, 2001). In effect for the C1 CO data, the artefact CO produced

422 from O₃ had contributed with unexpectedly high C¹⁷O abundances that led to the overestimated
423 δ¹³C(CO) analysed. The respective bias ¹³δ_b is quantified using

$$^{13}\delta_b = 7.26 \cdot 10^{-2} \Delta^{17}\text{O}(\text{CO}), \quad (\text{B1})$$

424 where the actual Δ¹⁷O(CO) value is approximated from the natural CO MIF signal ¹⁷Δ_n and the
425 typical O₃ MIF composition ¹⁷Δ_c as

$$\Delta^{17}\text{O}(\text{CO}) = ({}^{17}\Delta_n ([\text{CO}]_a - [\text{CO}]_c) + {}^{17}\Delta_c [\text{CO}]_c) ([\text{CO}]_a)^{-1}. \quad (\text{B2})$$

426 Here [CO]_a and [CO]_c denote the analysed CO mixing ratio and contamination magnitude, re-
427 spectively, used in the contamination assessment (see Appendix A, Eq. (A4)) and in calcula-
428 tions with the MM (see Sect. 3.1). For the purpose of the current estimate it is sufficient to take
429 ¹⁷Δ_n of +5‰ representing equilibrium enrichments expected in the remote free troposphere and
430 UT/LMS. For the O₃ MIF signature ¹⁷Δ_c, the value of +30‰ (the average Δ¹⁷O(O₃) expected
431 from the kinetic laboratory data at conditions met along the C1 flight routes, see Sect. 3.2 and
432 Table 1) is adopted. The coefficient that proportionates ¹³δ_b and Δ¹⁷O in Eq. (B1) is derived by
433 linearly regressing the δ¹³C(CO) biases (simulated using the calculation apparatus detailed by
434 Assonov and Brenninkmeijer, 2001) as a function of Δ¹⁷O(CO) varying within a (0–30)‰
435 range for the CO with initially unaccounted MIF (*e.g.*, the sample is assumed to be mass-
436 dependently fractionated). It therefore quantifies some extra +(0.726±0.003)‰ in the analysed
437 δ¹³C(CO) per every +10‰ of Δ¹⁷O(CO) excess. The most contaminated C1 WAS CO samples
438 at [O₃] above 300 nmol/mol are estimated to bear Δ¹⁷O(CO) of (6–12)‰ corresponding to frac-
439 tions of (0.10–0.27) of the artefact CO in the sample. Accordingly, the reckoned δ¹³C(CO) bi-
440 ases span (0.5–0.9)‰. Although not large, these well exceed the δ¹³C(CO) measurement preci-
441 sion of ±0.1‰ and were corrected for, and therefore are taken into account in the calculations
442 with the MM presented in Sect. 3.1.

443 **Acknowledgements**

444 [28] The authors are indebted to Claus Koepfel, Dieter Scharffe and Dr. Andreas Zahn for their
445 work and expertise on the carbon monoxide and ozone measurements in C1 and C2. Hella
446 Riede is acknowledged for comprehensive estimates of the species lifetimes along the
447 CARIBIC flight routes. We are grateful to Dr. Taku Umezawa, Dr. Angela K. Baker, Dr. Em-
448 ma C. Leedham, Dr. Sergey Assonov, the anonymous reviewer and Dr. Jan Kaiser for the help-
449 ful discussions and comments on the manuscript.

450 References

- 451 Assonov, S. S. and Brenninkmeijer, C. A. M.: A new method to determine the ^{17}O isotopic abundance in
 452 CO_2 using oxygen isotope exchange with a solid oxide, *Rapid Commun. Mass Spectrom.*, **15**,
 453 2426–2437, doi: [10.1002/rcm.529](https://doi.org/10.1002/rcm.529), 2001.
- 454 Assonov, S. S. and Brenninkmeijer, C. A. M.: A redetermination of absolute values for $^{17}\text{R}_{\text{VPDB-CO}_2}$ and
 455 $^{17}\text{R}_{\text{VSMOW}}$, *Rapid Commun. Mass Spectrom.*, **17**, 1017–1029, doi: [10.1002/Rcm.1011](https://doi.org/10.1002/Rcm.1011), 2003.
- 456 Assonov, S. S., Brenninkmeijer, C. A. M., Koeppel, C., and Röckmann, T.: CO_2 isotope analyses using
 457 large air samples collected on intercontinental flights by the CARIBIC Boeing 767,
 458 *Rapid Commun. Mass Spectrom.*, **23**, 822–830, doi: [10.1002/rcm.3946](https://doi.org/10.1002/rcm.3946), 2009.
- 459 Bhattacharya, S. K., Pandey, A., and Savarino, J.: Determination of intramolecular isotope distribution of
 460 ozone by oxidation reaction with silver metal, *J. Geophys. Res. Atm.*, **113**, D033303,
 461 doi: [10.1029/2006jd008309](https://doi.org/10.1029/2006jd008309), 2008.
- 462 Brenninkmeijer, C. A. M.: Measurement of the abundance of ^{14}CO in the atmosphere and the $^{13}\text{C}/^{12}\text{C}$ and
 463 $^{18}\text{O}/^{16}\text{O}$ ratio of atmospheric CO with applications in New Zealand and
 464 Antarctica, *J. Geophys. Res. Atm.*, **98**, 10595–10614, doi: [10.1029/93JD00587](https://doi.org/10.1029/93JD00587), 1993.
- 465 Brenninkmeijer, C. A. M., Müller, R., Crutzen, P. J., Lowe, D. C., Manning, M. R., Sparks, R. J., and van
 466 Velthoven, P. F. J.: A large ^{13}CO deficit in the lower Antarctic stratosphere due to “Ozone Hole”
 467 Chemistry: Part I, Observations, *Geophys. Res. Lett.*, **23**, 2125–2128, doi: [10.1029/96gl01471](https://doi.org/10.1029/96gl01471), 1996.
- 468 Brenninkmeijer, C. A. M. and Röckmann, T.: Principal factors determining the $^{18}\text{O}/^{16}\text{O}$ ratio of
 469 atmospheric CO as derived from observations in the southern hemispheric troposphere and lowermost
 470 stratosphere, *J. Geophys. Res. Atm.*, **102**, 25477–25485, doi: [10.1029/97JD02291](https://doi.org/10.1029/97JD02291), 1997.
- 471 Brenninkmeijer, C. A. M., Crutzen, P. J., Fischer, H., Gusten, H., Hans, W., Heinrich, G.,
 472 Heintzenberg, J., Hermann, M., Immelmann, T., Kersting, D., Maiss, M., Nolle, M., Pitscheider, A.,
 473 Pohlkamp, H., Scharffe, D., Specht, K., and Wiedensohler, A.: CARIBIC – Civil aircraft for global
 474 measurement of trace gases and aerosols in the tropopause region, *J. Atmos. Oceanic Technol.*, **16**,
 475 1373–1383, doi: [10.1175/1520-0426\(1999\)016<1373:Ccafgm>2.0.Co;2](https://doi.org/10.1175/1520-0426(1999)016<1373:Ccafgm>2.0.Co;2), 1999.
- 476 Brenninkmeijer, C. A. M., Koeppel, C., Röckmann, T., Scharffe, D. S., Bränlich, M., and Gros, V.:
 477 Absolute measurement of the abundance of atmospheric carbon monoxide, *J. Geophys. Res. Atm.*, **106**,
 478 10003–10010, doi: [10.1029/2000jd900342](https://doi.org/10.1029/2000jd900342), 2001.
- 479 Brenninkmeijer, C. A. M., Janssen, C., Kaiser, J., Röckmann, T., Rhee, T. S., and Assonov, S. S.: Isotope
 480 effects in the chemistry of atmospheric trace compounds, *Chem. Rev.*, **103**, 5125–5161,
 481 doi: [10.1021/Cr020644k](https://doi.org/10.1021/Cr020644k), 2003.
- 482 Brenninkmeijer, C. A. M., Crutzen, P., Boumard, F., Dauer, T., Dix, B., Ebinghaus, R., Filippi, D.,
 483 Fischer, H., Franke, H., Frieß, U., Heintzenberg, J., Helleis, F., Hermann, M., Kock, H. H.,
 484 Koeppel, C., Lelieveld, J., Leuenberger, M., Martinsson, B. G., Miemczyk, S., Moret, H. P.,
 485 Nguyen, H. N., Nyfeler, P., Oram, D., O'Sullivan, D., Penkett, S., Platt, U., Pupek, M., Ramonet, M.,
 486 Randa, B., Reichelt, M., Rhee, T. S., Rohwer, J., Rosenfeld, K., Scharffe, D., Schlager, H.,
 487 Schumann, U., Slemr, F., Sprung, D., Stock, P., Thaler, R., Valentino, F., van Velthoven, P.,
 488 Waibel, A., Wandel, A., Waschitschek, K., Wiedensohler, A., Xueref-Remy, I., Zahn, A.,
 489 Zech, U., and Ziereis, H.: Civil Aircraft for the regular investigation of the atmosphere based on an
 490 instrumented container: The new CARIBIC system, *Atmos. Chem. Phys.*, **7**, 4953–4976,
 491 doi: [10.5194/acp-7-4953-2007](https://doi.org/10.5194/acp-7-4953-2007), 2007.

492 Coplen, T. B.: Reporting of stable hydrogen, carbon, and oxygen isotopic abundances (Technical Report),
493 *Pure Appl. Chem.*, **66**, 273–276, doi: [10.1351/pac199466020273](https://doi.org/10.1351/pac199466020273), 1994.

494 Craig, H.: Isotopic standards for carbon and oxygen and correction factors for mass-spectrometric analysis
495 of carbon dioxide, *Geochim. Cosmochim. Acta*, **12**, 133–149, doi: [10.1016/0016-7037\(57\)90024-8](https://doi.org/10.1016/0016-7037(57)90024-8),
496 1957.

497 Gonfiantini, R.: Standards for Stable Isotope Measurements in Natural Compounds, *Nature*, **271**,
498 534–536, 1978.

499 Gromov, S., Jöckel, P., Sander, R., and Brenninkmeijer, C. A. M.: A kinetic chemistry tagging technique
500 and its application to modelling the stable isotopic composition of atmospheric trace gases,
501 *Geosci. Model Dev.*, **3**, 337–364, doi: [10.5194/gmd-3-337-2010](https://doi.org/10.5194/gmd-3-337-2010), 2010.

502 Guenther, J., Erbacher, B., Krankowsky, D., and Mauersberger, K.: Pressure dependence of two relative
503 ozone formation rate coefficients, *Chem. Phys. Lett.*, **306**, 209–213,
504 doi: [10.1016/S0009-2614\(99\)00469-8](https://doi.org/10.1016/S0009-2614(99)00469-8), 1999.

505 Janssen, C., Guenther, J., Krankowsky, D., and Mauersberger, K.: Temperature dependence of ozone rate
506 coefficients and isotopologue fractionation in ^{16}O – ^{18}O oxygen mixtures, *Chem. Phys. Lett.*, **367**,
507 34–38, doi: [10.1016/S0009-2614\(02\)01665-2](https://doi.org/10.1016/S0009-2614(02)01665-2), 2003.

508 Janssen, C.: Intramolecular isotope distribution in heavy ozone ($^{16}\text{O}^{18}\text{O}^{16}\text{O}$ and $^{16}\text{O}^{16}\text{O}^{18}\text{O}$),
509 *J. Geophys. Res. Atm.*, **110**, D08308, doi: [10.1029/2004jd005479](https://doi.org/10.1029/2004jd005479), 2005.

510 Johnston, J. C. and Thiemens, M. H.: The isotopic composition of tropospheric ozone in three
511 environments, *J. Geophys. Res. Atm.*, **102**, 25395–25404, doi: [10.1029/97jd02075](https://doi.org/10.1029/97jd02075), 1997.

512 Krankowsky, D., Bartecki, F., Klees, G. G., Mauersberger, K., Schellenbach, K., and Stehr, J.:
513 Measurement of heavy isotope enrichment in tropospheric ozone, *Geophys. Res. Lett.*, **22**, 1713–1716,
514 doi: [10.1029/95gl01436](https://doi.org/10.1029/95gl01436), 1995.

515 Krankowsky, D., Lämmerzahl, P., Mauersberger, K., Janssen, C., Tuzson, B., and Röckmann, T.:
516 Stratospheric ozone isotope fractionations derived from collected samples, *J. Geophys. Res. Atm.*, **112**,
517 D08301, doi: [10.1029/2006jd007855](https://doi.org/10.1029/2006jd007855), 2007.

518 Li, W., Gibbs, G. V., and Oyama, S. T.: Mechanism of Ozone Decomposition on a Manganese Oxide
519 Catalyst. 1. In Situ Raman Spectroscopy and Ab Initio Molecular Orbital
520 Calculations, *J. Am. Chem. Soc.*, **120**, 9041–9046, doi: [10.1021/ja981441+](https://doi.org/10.1021/ja981441+), 1998.

521 Mauersberger, K.: Measurement of Heavy Ozone in the Stratosphere, *Geophys. Res. Lett.*, **8**, 935–937,
522 doi: [10.1029/G1008i008p00935](https://doi.org/10.1029/G1008i008p00935), 1981.

523 McNaught, A. D. and Wilkinson, A.: IUPAC. Compendium of Chemical Terminology (the "Gold Book"),
524 XML on-line corrected version: <http://goldbook.iupac.org> (2006-) created by
525 M. Nic, J. Jirat, B. Kosata; updates compiled by A. Jenkins, doi: [10.1351/goldbook.O04322](https://doi.org/10.1351/goldbook.O04322), 1997.

526 Natrella, M.: NIST/SEMATECH e-Handbook of Statistical Methodsed., edited by: Croarkin, C. and
527 Tobias, P., NIST/SEMATECH, <http://www.itl.nist.gov/div898/handbook/> (last access: 07 May 2014),
528 2003.

529 Novelli, P. C., Masarie, K. A., and Lang, P. M.: Distributions and recent changes of carbon monoxide in
530 the lower troposphere, *J. Geophys. Res.*, **103**, 19015–19033, doi: [10.1029/98jd01366](https://doi.org/10.1029/98jd01366), 1998.

531 Novelli, P. C., Masarie, K. A., Lang, P. M., Hall, B. D., Myers, R. C., and Elkins, J. W.: Reanalysis of
532 tropospheric CO trends: Effects of the 1997–1998 wildfires, *J. Geophys. Res.*, **108**, 4464,
533 doi: [10.1029/2002jd003031](https://doi.org/10.1029/2002jd003031), 2003.

- 534 Oyama, S. T.: Chemical and Catalytic Properties of Ozone, *Catal. Rev. Sci. Eng.*, **42**, 279–322,
535 doi: [10.1081/cr-100100263](https://doi.org/10.1081/cr-100100263), 2000.
- 536 Pan, L. L., Randel, W. J., Gary, B. L., Mahoney, M. J., and Hints, E. J.: Definitions and sharpness of the
537 extratropical tropopause: A trace gas perspective, *J. Geophys. Res. Atm.*, **109**, D23103,
538 doi: [10.1029/2004jd004982](https://doi.org/10.1029/2004jd004982), 2004.
- 539 Röckmann, T., Brenninkmeijer, C. A. M., Neeb, P., and Crutzen, P. J.: Ozonolysis of nonmethane
540 hydrocarbons as a source of the observed mass independent oxygen isotope enrichment in tropospheric
541 CO, *J. Geophys. Res. Atm.*, **103**, 1463–1470, doi: [10.1029/97JD02929](https://doi.org/10.1029/97JD02929), 1998a.
- 542 Röckmann, T., Brenninkmeijer, C. A. M., Saueressig, G., Bergamaschi, P., Crowley, J. N.,
543 Fischer, H., and Crutzen, P. J.: Mass-independent oxygen isotope fractionation in atmospheric CO as a
544 result of the reaction CO+OH, *Science*, **281**, 544–546, doi: [10.1126/science.281.5376.544](https://doi.org/10.1126/science.281.5376.544), 1998b.
- 545 Röckmann, T., Jöckel, P., Gros, V., Bräunlich, M., Possnert, G., and Brenninkmeijer, C. A. M.: Using ¹⁴C,
546 ¹³C, ¹⁸O and ¹⁷O isotopic variations to provide insights into the high northern latitude surface CO
547 inventory, *Atmos. Chem. Phys.*, **2**, 147–159, doi: [10.5194/acp-2-147-2002](https://doi.org/10.5194/acp-2-147-2002), 2002.
- 548 Savarino, J., Bhattacharya, S. K., Morin, S., Baroni, M., and Doussin, J. F.: The NO+O₃ reaction: A triple
549 oxygen isotope perspective on the reaction dynamics and atmospheric implications for the transfer of
550 the ozone isotope anomaly, *J. Chem. Phys.*, **128**, 194303, doi: [10.1063/1.2917581](https://doi.org/10.1063/1.2917581), 2008.
- 551 Savarino, J. and Morin, S.: The N, O, S Isotopes of Oxy-Anions in Ice Cores and Polar Environments, in:
552 Handbook of Environmental Isotope Geochemistry, edited by: Baskaran, M., Advances in Isotope
553 Geochemistry, Springer Berlin Heidelberg, 835–864, 2012.
- 554 Scharffe, D., Slemr, F., Brenninkmeijer, C. A. M., and Zahn, A.: Carbon monoxide measurements onboard
555 the CARIBIC passenger aircraft using UV resonance fluorescence, *Atmos. Meas. Tech.*, **5**, 1753–1760,
556 doi: [10.5194/amt-5-1753-2012](https://doi.org/10.5194/amt-5-1753-2012), 2012.
- 557 Schinke, R., Grebenshchikov, S. Y., Ivanov, M. V., and Fleurat-Lessard, P.: Dynamical Studies Of The
558 Ozone Isotope Effect: A Status Report, *Annu. Rev. Phys. Chem.*, **57**, 625–661,
559 doi: [10.1146/annurev.physchem.57.032905.104542](https://doi.org/10.1146/annurev.physchem.57.032905.104542), 2006.
- 560 Stevens, C. M., Kaplan, L., Gorse, R., Durkee, S., Compton, M., Cohen, S., and Bielling, K.: The Kinetic
561 Isotope Effect for Carbon and Oxygen in the Reaction CO+OH, *Int. J. Chem. Kinet.*, **12**, 935–948,
562 doi: [10.1002/kin.550121205](https://doi.org/10.1002/kin.550121205), 1980.
- 563 Vicars, W. C., Bhattacharya, S. K., Erbland, J., and Savarino, J.: Measurement of the ¹⁷O-excess ($\Delta^{17}\text{O}$) of
564 tropospheric ozone using a nitrite-coated filter, *Rapid Commun. Mass Spectrom.*, **26**, 1219–1231,
565 doi: [10.1002/rcm.6218](https://doi.org/10.1002/rcm.6218), 2012.
- 566 Vicars, W. C. and Savarino, J.: Quantitative constraints on the ¹⁷O-excess ($\Delta^{17}\text{O}$) signature of surface
567 ozone: Ambient measurements from 50°N to 50°S using the nitrite-coated filter technique,
568 *Geochim. Cosmochim. Acta*, **135**, 270–287, doi: [10.1016/j.gca.2014.03.023](https://doi.org/10.1016/j.gca.2014.03.023), 2014.
- 569 Zahn, A., Brenninkmeijer, C. A. M., Maiss, M., Scharffe, D. H., Crutzen, P. J., Hermann, M.,
570 Heintzenberg, J., Wiedensohler, A., Güsten, H., Heinrich, G., Fischer, H., Cuijpers, J. W. M., and van
571 Velthoven, P. F. J.: Identification of extratropical two-way troposphere-stratosphere mixing based on
572 CARIBIC measurements of O₃, CO, and ultrafine particles, *J. Geophys. Res.*, **105**, 1527–1535,
573 doi: [10.1029/1999jd900759](https://doi.org/10.1029/1999jd900759), 2000.
- 574 Zahn, A., Brenninkmeijer, C. A. M., Asman, W. A. H., Crutzen, P. J., Heinrich, G., Fischer, H.,
575 Cuijpers, J. W. M., and van Velthoven, P. F. J.: Budgets of O₃ and CO in the upper troposphere:

- 576 CARIBIC passenger aircraft results 1997–2001, *J. Geophys. Res. Atm.*, **107**, 4337,
 577 doi: [10.1029/2001jd001529](https://doi.org/10.1029/2001jd001529), 2002.
- 578 Zahn, A., Weppner, J., Widmann, H., Schlote-Holubek, K., Burger, B., Kühner, T., and Franke, H.: A fast
 579 and precise chemiluminescence ozone detector for eddy flux and airborne application,
 580 *Atmos. Meas. Tech.*, **5**, 363–375, doi: [10.5194/amt-5-363-2012](https://doi.org/10.5194/amt-5-363-2012), 2012.

581 Tables

582 Table 1. Ozone $^{18}\text{O}/^{16}\text{O}$ isotope ratios from literature and this study

| Domain | T (K) | P (hPa) | $\delta^{18}\text{O}(\text{O}_3)$ (‰) | Remarks |
|--------------|---------|---------|---------------------------------------|---------|
| Stratosphere | 190–210 | 13–50 | 83–93 (<3) | 1 |
| UT/LMS | 220–235 | 240–270 | 89–95 (8) | 2 |
| | | | 84–88 (6) | T |
| | | | 91–98 (9) | TC |
| | | | 112–124 (17) | C |
| Laboratory | 190–210 | 67 | 87–97 (6) | 3 |
| | 220–235 | 67 | 102–110 (6) | 3 |
| | 220–235 | 240–270 | 95–103 | 4 |

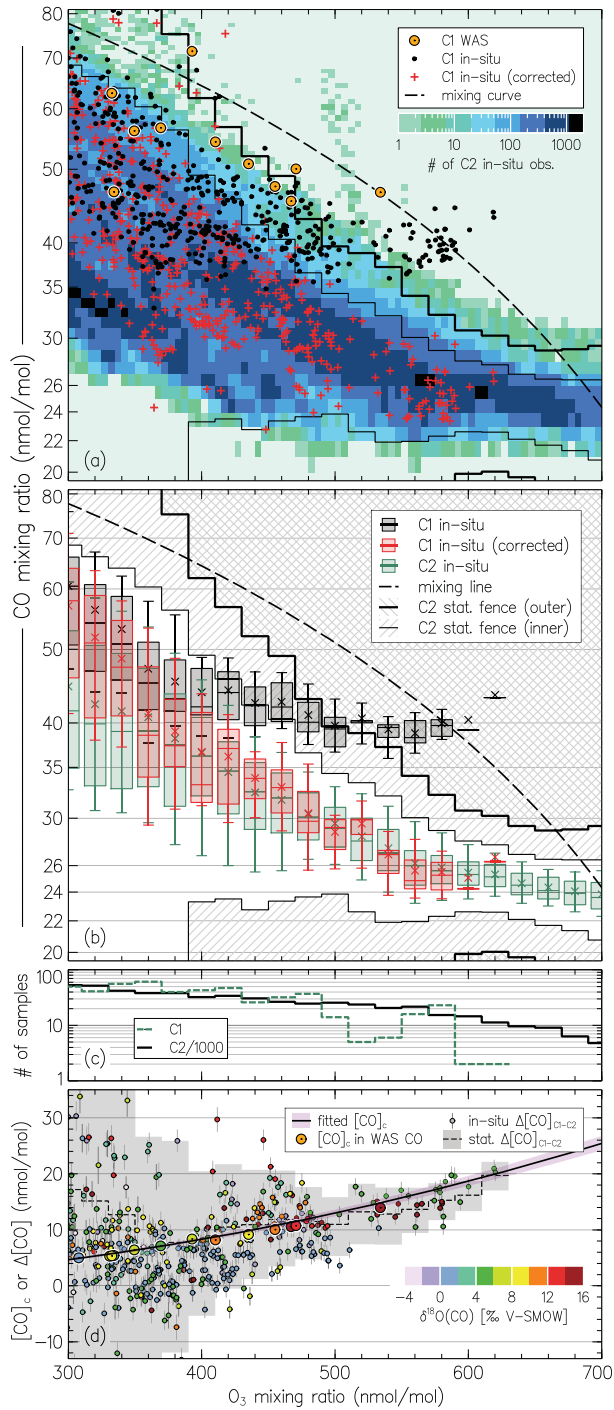
Notes: Values in parentheses denote the average of the estimates' standard errors. The expected O_3 isotope composition on the VSMOW scale is calculated from the O_3 enrichments reported relative to O_2 using $\delta^{18}\text{O}(\text{O}_3)_{\text{VSMOW}} = \delta^{18}\text{O}(\text{O}_2)_{\text{VSMOW}} + {}^{18}\delta(\text{O}_3)_{\text{Air-O}_2} + [\delta^{18}\text{O}(\text{O}_2)_{\text{VSMOW}} \times {}^{18}\epsilon(\text{O}_3)_{\text{Air-O}_2}]$.

¹ Observations (see Krankowsky *et al.* (2007) and refs. therein), lowermost values (19–25 km). Quoted temperature range is derived by matching measured $\delta^{18}\text{O}(\text{O}_3)$ and laboratory data (see note ³).

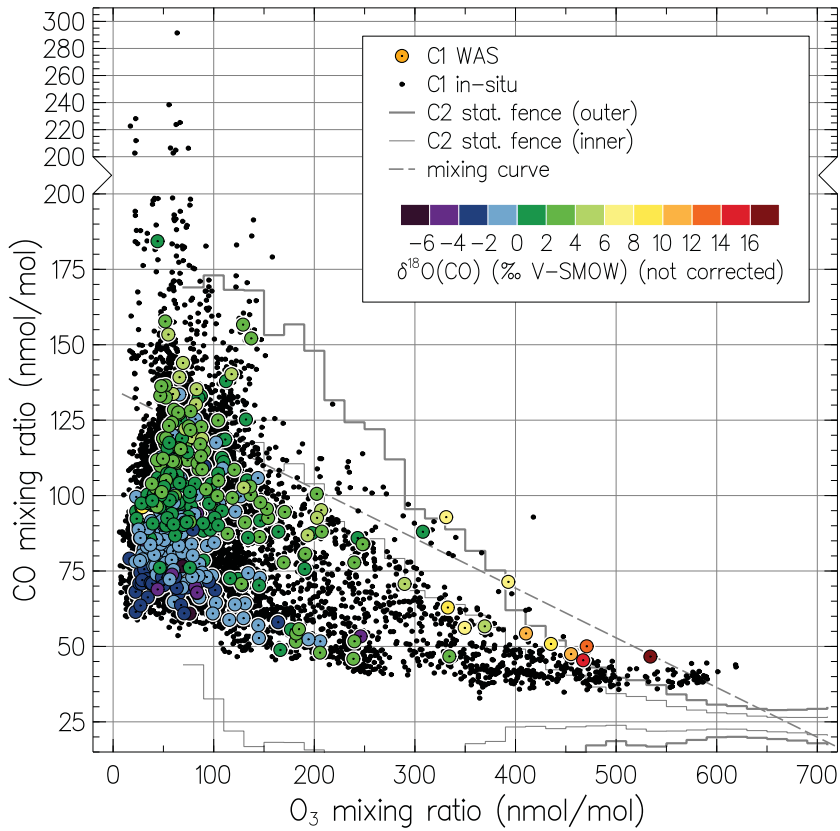
² This study, C1 observations (10–12 km). Letters denote the estimates derived using the data from Bhattacharya *et al.* (2008) and assuming only terminal (T), only central (C) and equiprobable terminal and central (TC) O_3 atoms transfer to the artefact CO .

³ Calculated using the laboratory KIE temperature dependence data summarised by Janssen *et al.* (2003).

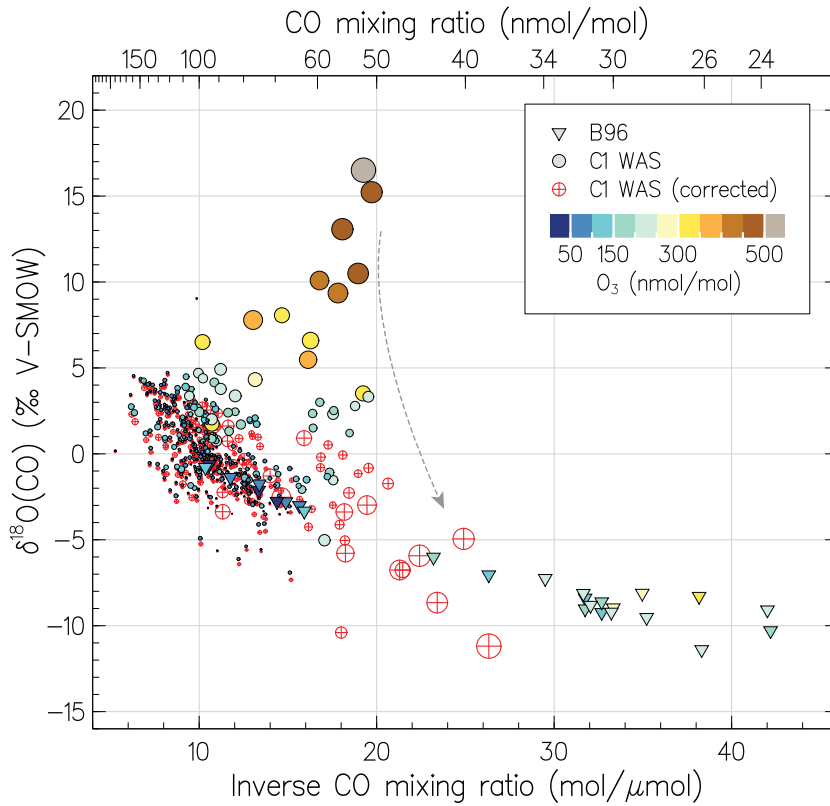
⁴ Calculated assuming a pressure dependence of the O_3 formation KIE similar to that measured at 320 K (see Guenther *et al.* (1999) and refs. therein).



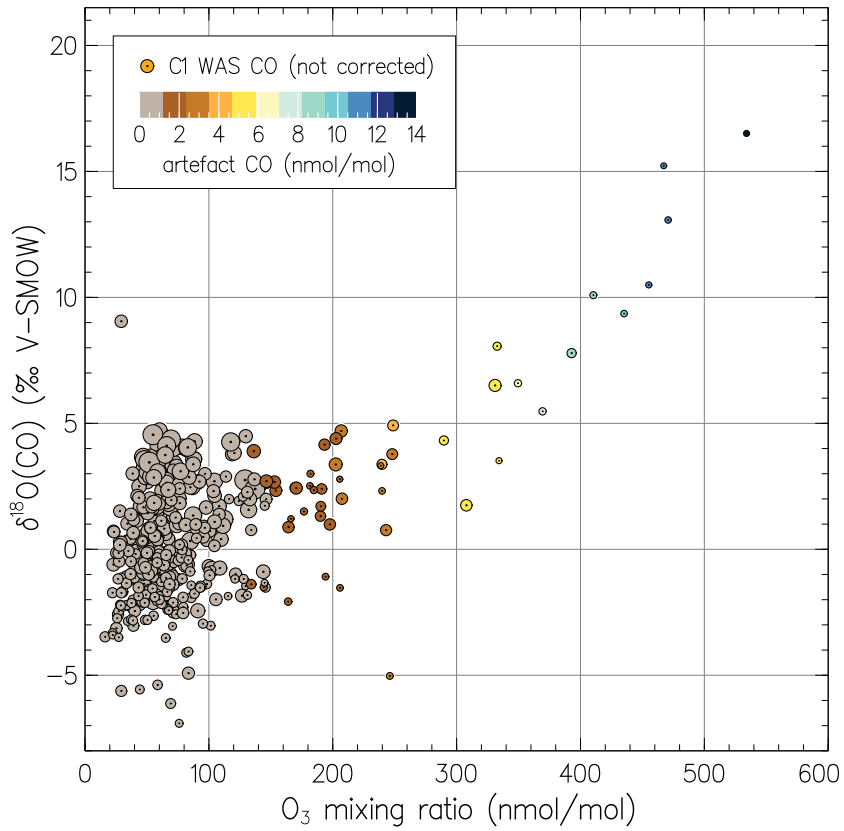
584 Fig. 1. (a) Distribution of CO mixing ratios as a function of concomitant O₃ mixing ratios measured by
585 CARIBIC in the LMS ([O₃] > 300 nmol/mol). The shaded area is the two-dimensional histogram of the C2
586 measurements (all C2 data obtained until June 2013) counted in 5 × 1 nmol/mol size [O₃] × [CO] bins, thus
587 darker areas emphasise greater numbers of particular CO–O₃ pairs observed. Small symbols denote the
588 original C1 *in situ* measurements (black) and corrected for the artefacts (red); the C1 WAS analyses (11 of
589 total 408) are shown with large symbols. Thin and thick step-lines demark the inner and outer statistical
590 fences (ranges outside which the data points are considered mild or extreme outliers, see text) of the C2
591 data, respectively. The dashed curve exemplifies compositions expected from the linear mixing of very
592 different (*e.g.*, tropospheric and stratospheric) end-members. (b) Statistics on CO mixing ratios from C1
593 and C2 data shown in box-and-whisker diagrams for samples clustered in 20 nmol/mol O₃ bins (whiskers
594 represent 9th/91st percentiles). (c) Sample statistic for each CARIBIC dataset (note the C2 figures scaled
595 down by a factor of 1000). (d) Estimates of the C1 *in situ* CO contamination strength [CO]_c as a function
596 of [O₃] (solid line) obtained by fitting the difference Δ[CO] between the C2 and C1 *in situ* [CO] (small
597 symbols) as detailed in Appendix A (Eq. (A2)). Step line shows the Δ[CO] for the statistical averages (the
598 shaded area equals the height of the inner statistical fences of the C2 data). Large symbols denote the es-
599 timates of C_c in the C1 WAS data (slight variations *vs.* the *in situ* data are due to the sample mixing ef-
600 fects, see Sect. 3). Colour denotes the respective C1 WAS δ¹⁸O(CO) (note that typically 6–7 *in situ* meas-
601 urements correspond to one WAS sample).



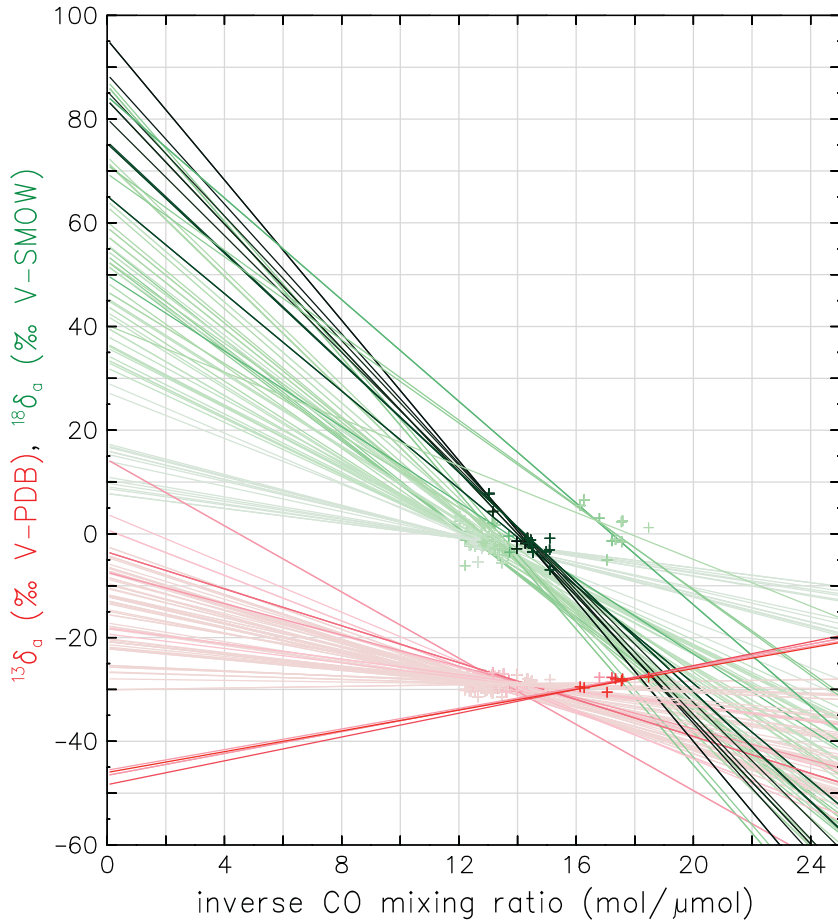
602 Fig. 2. (accompanies Fig. 1) Carbon monoxide and ozone mixing ratios measured in C1. Small black sym-
 603 bols denote the C1 *in situ* measurements ($n = 12753$). The C1 WAS analyses ($n = 408$) are shown with
 604 large symbols; colour denotes the concomitant $\delta^{18}\text{O}(\text{CO})$ measurements. Thin and thick step-lines denote
 605 the inner and outer statistical fences of the C2 data, respectively. The dashed curve exemplifies composi-
 606 tions expected from the linear mixing of tropospheric and stratospheric end-members (see caption to Fig. 1
 607 for details).



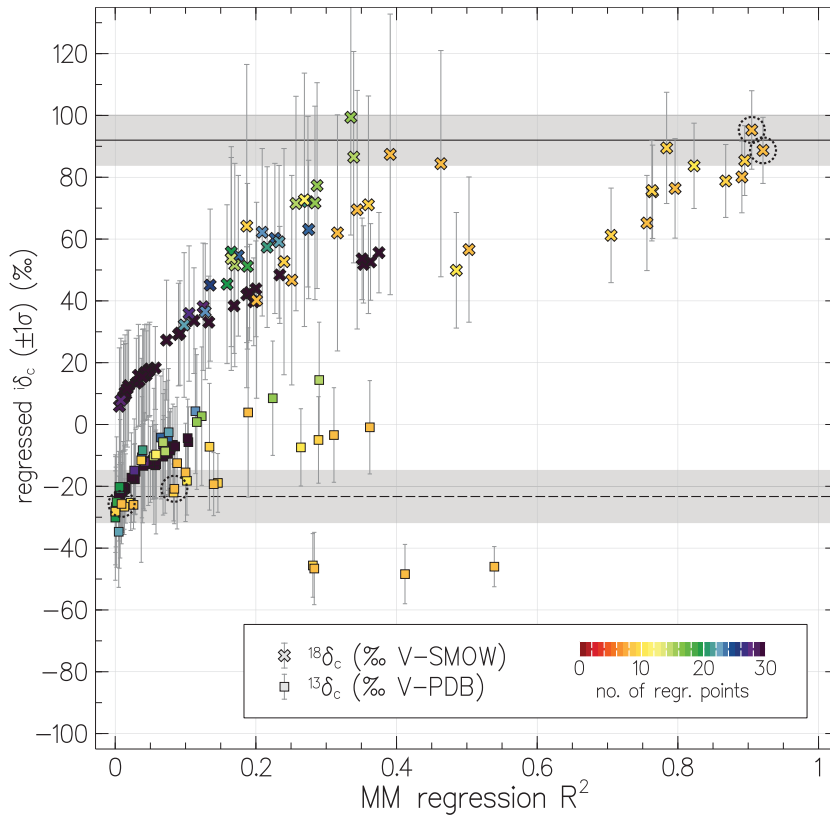
608 Fig. 3. $^{18}\text{O}/^{16}\text{O}$ isotope composition of CO as a function of its reciprocal mixing ratio. Triangles present
 609 the data from the remote SH UT/LMS obtained by Brenninkmeijer *et al.* (1996) (B96). Colour refers to the
 610 concomitantly observed O_3 abundances; note the extremely low $[\text{O}_3]$ encountered by B96 in the Antarctic
 611 "ozone hole" conditions. Filled and hollow circles denote the original and corrected (as exemplified by the
 612 dashed arrow) C1 WAS data, respectively, with the symbol size scaling proportional to the estimated con-
 613 tamination magnitude (see text).



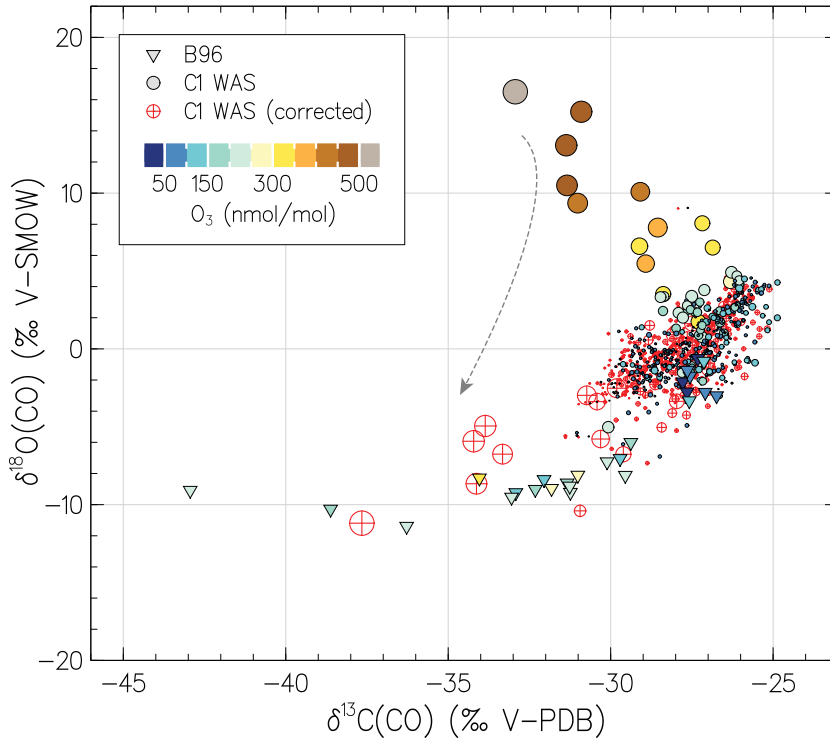
614 Fig. 4. Measured C1 WAS $\delta^{18}\text{O}(\text{CO})$ (not corrected for artefacts) as a function of concomitant O_3 mixing
 615 ratio. Symbol colour denotes the artefact CO component (integral $[\text{CO}]_c$ per each WAS); symbol size
 616 scales proportionally to the WAS CO mixing ratio corrected for artefacts (see Sect. 3 for details).



617 Fig. 5. Keeling plot of the data used in the calculations with the mixing model (MM). The C1 WAS iso-
 618 tope CO measurements are shown with symbols, solid lines denote the linear regressions through the vari-
 619 ous sets of samples selected by the MM ($n = 80$ sets are plotted). Colours refer to the $\delta^{13}\text{C}$ (red) and $\delta^{18}\text{O}$
 620 (green) data, colour intensity indicates the coefficient of determination (R^2) of each regression, respec-
 621 tively. Darker colours denote higher R^2 values, with maxima of 0.92 for $\delta^{18}\text{O}$ and 0.54 for $\delta^{13}\text{C}$ data, respec-
 622 tively. The inferred contamination signatures (δ_c) are found at $([\text{CO}]_a)^{-1} \rightarrow 0$. Regression uncertainties are
 623 shown in Fig. 6. Note that because different subsets of samples contain same data points, some of the
 624 symbols are plotted over (*i.e.*, not all symbols contributing to a particular regression case may be seen).



625 Fig. 6. Results of the regression calculation with the MM. Shown with symbols are the contamination
 626 source isotope signatures $i\delta_c$ as a function of the respective coefficient of determination (R^2). Colour de-
 627 notes the number of samples in each subset selected. Solid and dashed lines present the best guess
 628 ± 1 standard deviation of the mean for the $^{18}\delta_c$ and $^{13}\delta_c$ estimates. Dashed circles mark the estimates ob-
 629 tained at highest R^2 for $^{18}\delta_c$ regression (above 0.9). See text for details.



630 Fig. 7. $^{18}\text{O}/^{16}\text{O}$ and $^{13}\text{C}/^{12}\text{C}$ isotope composition of CO measured in C1. Triangles present the data from the
 631 remote SH UT/LMS obtained by Brenninkmeijer *et al.* (1996) (B96). Colour refers to the concomitantly
 632 observed O_3 abundances; note the extremely low $[\text{O}_3]$ encountered by B96 in the Antarctic ozone-hole
 633 conditions. Filled and hollow circles denote the original and corrected (as exemplified by the dashed ar-
 634 row) C1 WAS data, respectively, with the symbol size scaling proportional to the estimated contamination
 635 magnitude (see text for details).